Optimal cascade operation of optical phased-array beam deflectors

James A. Thomas and Yeshaiahu Fainman

An optimal strategy for cascading phased-array deflectors is presented that allows for high-resolution random-access beam steering with continuous scan-angle control but requires a minimum number of control lines. The system is analyzed theoretically by use of a Fourier optics approach and then verified experimentally. A pair of 32-channel optical phased arrays fabricated by use of surface electrodes on lanthanum-modified lead zirconate titanate (PLZT) was sandwiched together to form a functional two-stage phased-array cascade. Experimental results from the PLZT-based two-stage deflector are presented that confirm the performance enhancements of the optimized cascading technique. A phase-staggered discrete–offset-bias protocol for controlling the cascaded system is shown to be optimal in terms of maximum diffraction efficiency and minimum number of control lines, while still providing for full analog scan control.

OCIS codes: 050.0080, 070.0030, 230.0080, 120.0380, 110.0180.

1. Introduction

A multitude of useful static optical functions can be achieved with diffractive optical elements (DOE's), including beam deflection, anamorphic lensing, array generation, and aberration correction. These operations are achieved by the imposition of particular phase profiles on an incident wave front. Performing such DOE functions in a dynamic fashion is the goal of an emerging optical phased-array technology.[1] Optical phased arrays are direct functional analogs of microwave phased-array antennas[2] that allow agile, inertialess steering of microwave beams. The optical arrays mimic the behavior of passive, space-fed microwave phased-array systems that have been scaled down for use at optical wavelengths and thus share the same fundamental beam-forming concepts as their microwave precursors.

Optical phased arrays provide an elegant means for the inertialess, high-resolution random-access beam steering that is required by numerous applications, including laser radar, laser communication, and laser projection display. For such applications high-resolution scanners with large apertures are needed to provide a precision pointing capability for light beams with potentially high light power. Typical specifications call for more than 10^4 addressable points, which in turn requires at least an equal number of independently controlled phase modulators in the array.[3] Numerous line-management techniques have been explored to reduce the number of control lines required to regulate fully such a phased-array deflector while still providing continuous scan-angle control. Cascading phased arrays in tandem offers a good solution to this problem. With careful design of the cascade architecture and proper choice of the phased-array programming strategy, one can achieve full scan control with optimal diffraction efficiency (DE) by using a minimum number of control lines.

An optical phased array is typically composed of a multichannel array of electro-optic (E-O) phase modulators (see Fig. 1). However, because of the general need for small far-field spot patterns scannable over a large angular range (i.e., a large device aperture with small modulator sizes), optical phased arrays can require an enormous number of individual phase shifters. Previous research (Ref. 1) has described some basic methods for reducing the interconnections required for high-resolution phased-array deflectors. These include the restriction to one-dimensional (1-D) arrays for separate X–Y beam deflection and the implementation of a simple coarse–fine cascading scheme. The present paper specifically analyzes the problem of addressing large 1-D arrays of phase mod-

The authors are with the Department of Electrical and Computer Engineering, University of California at San Diego, La Jolla, California 92093-0407.

Received 26 March 1998; revised manuscript received 24 June 1998.

0003-6935/98/266196-17$15.00/0

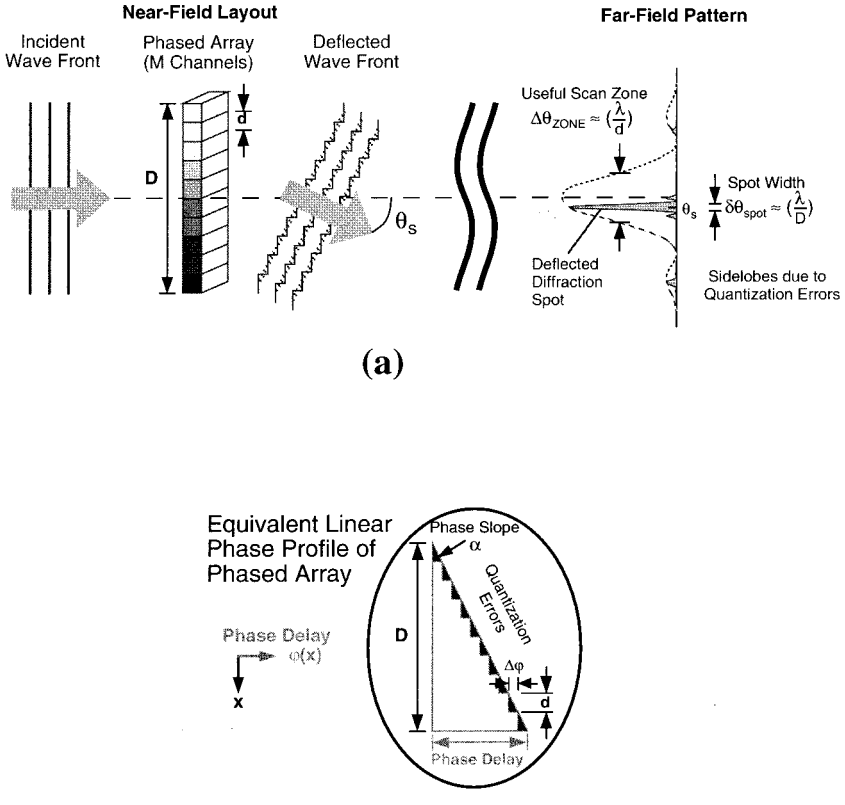

Fig. 1. Basic concept of a 1-D phased-array deflector: (a) near-field layout and far-field intensity pattern, and (b) equivalent phase profile of the 1-D array (with unfolded phases). Quantization errors are shown as dark notches.

ulators used for beam deflection and describes an alternative cascading solution with improved performance. Experiments with optical phased-array deflectors fabricated by use of lanthanum-modified lead zirconate titanate (PLZT) are described that confirm the usefulness of our approach. The specific attributes and implementation of this new optimal cascading scheme are discussed in the following sections.

The outline of this paper is as follows. In Section 2 we present a brief review of earlier optical phased-array systems and discuss the addressing techniques used in these systems. The majority of this paper then deals with presenting a Fourier based theoretical analysis of cascaded optical phased-array deflectors and associated experiments with PLZT-based phased-array devices that corroborate the theory. Section 3 is devoted to a theoretical description of a single-stage phased-array deflector by use of Fourier optics analysis, and several key features of the basic deflector are pointed out. Section 4 introduces the general concepts behind a two-stage phased-array deflector. In Section 5 the Fourier analysis of Section 3 is extended to modeling an aligned two-stage phased-array cascade. Here the key attributes of the two stages are pointed out, and the optimal programming strategy for such a cascaded array deflector is determined. In Section 6 we describe the design and implementation of two 32-channel optical phased arrays that use PLZT and show the experimentally observed outputs from the two-stage deflector. The observed data support the theoretical description of Section 5. The overall results are then summarized in Section 6.

2. Background

Several forms of optical phased arrays have been developed in the past by use of various designs in a wide variety of E-O materials for phase modulation. As early as 1971, Meyer[4] demonstrated a multichannel array of bulk lithium tantalate modulators for optical beam deflection. The deflector consisted of 46 phase shifters in a 1-D geometry, and independent control lines were provided for each channel to obtain continuous scan control. Several fundamental concepts of optical phased-array deflection were verified by this simple single-stage device. Shortly thereafter, Ninomiya[5] demonstrated a phased array of bulk-prism deflecting elements made with lithium niobate. This device exploited an array concept primarily to enhance the deflector resolution beyond that of a single deflecting element. In further research to simplify the device design, Ninomiya[6] introduced a novel two-stage arrangement that included offset phase electrodes set in front of each prismlike deflecting element. This allowed the phased array to create a phase-staggered approximation to an arbitrary linear

phase profile, hence providing continuous deflection-angle control while maintaining enhanced resolution. (Lee and Zook[7] described a similar cascade arrangement for resolution enhancement in a less openly disclosed patent issued in 1972.)

Later efforts led to the design of fast, high-performance 1-D phased-array beam deflectors that use integrated-optics AlGaAs channel waveguides.[8–10] Vasey *et al.*[10] reported a 50-element rib waveguide device that exploited an integrated two-stage configuration analogous to Ninomiya's arrangement. In this device a pair of sawtooth-shaped electrodes across the array of waveguides creates a sequence of identical prismlike deflecting elements that, by themselves, form a discrete-state scanner. Separate block electrodes were placed in front of the primary electrodes as in the Ninomiya design so that continuous beam steering could be achieved. This layout greatly reduced the number of electrical connections required by the 50-channel array.

McManamon *et al.*[1] recently developed compact, high-resolution optical phased arrays based on a nematic liquid crystal. These arrays have a large aperture (4 cm $\times$ 4 cm) and contain up to 43,000 phase modulators. To alleviate the burden of addressing such a large number of modulators while maintaining continuous scan control, McManamon *et al.* used a two-stage coarse–fine cascade arrangement for the phased arrays. The coarse stage performs broad, discrete deflection, and the fine stage produces continuous angular deflection over a narrow range. The two stages are designed so that, when combined, they yield continuous scan-angle coverage. The coarse stage is formed from a large phased array by use of a reduced-leadout addressing architecture in which the modulators in the large array are interconnected to form a sequence of identical subarrays (see Refs. 1 and 11). In the prototypical coarse deflector that contained 43,008 modulators, only 256 control lines were required to address the full array because 256 modulators were grouped into each subarray. The fine deflector stage contained 512 independently controlled modulators. This coarse–fine cascading strategy requires far fewer control lines than does a fully addressed single-stage phased array but possesses the full flexibility of a single-stage deflector.

An optical solid-state phased array designed for potentially high-speed operation with PLZT was recently demonstrated.[12] This single-stage phased-array device is capable of fast, continuous scanning but requires relatively high drive voltages. Cascading was examined here as a means of reducing the control-line counts, hence to reduce the number of high-voltage drivers required. A coarse–fine cascading structure was initially considered for the PLZT phased arrays, but it was found that the Ninomiya scheme could also be applied to such phased-array deflectors and would offer better performance attributes. This paper presents these new results.

It should finally be noted that other techniques can reduce the line counts of phased-array deflectors without the use of cascading. Talbot and Song[13] suggested using fixed resistive networks between electrodes in a single-stage phased-array deflector to achieve a simple two- or three-terminal device. Similar arrangements have been used in phased arrays dedicated as variable-focal-length lenses.[14,15] Such schemes necessarily require that the E-O medium exhibit perfect linear or quadratic behavior over the full range of voltages dropped between electrodes, and they cannot fully compensate for changes in E-O behavior arising from aging or material saturation because the resistance values are fixed. Furthermore, in these schemes the phase modulators must be capable of higher-order (i.e., greater than 2π) phase shifts because the fixed resistive networks cannot provide for 2π phase resets in the array programming. This places severe constraints on the modulators. The line-count reduction techniques accomplished through cascading can indeed perform active E-O device compensation and, in the case of piston-type phase shifters, require no more than 2π rad of phase shift from any single modulator.

3. Phased-Array Beam-Steering Theory

An optical phased array can steer an incident beam by an angle θ_S by approximation of an ideal thin prism with a continuous linear phase function $\phi_{\text{prism}}(x) = \alpha x$, where $\alpha = (2\pi/\lambda)\sin(\theta_S)$, λ is the wavelength of the optical beam, and θ_S is the specified deflection angle. The output of the deflector is found in the far-field diffraction pattern of the array [see Fig. 1(a)]. Because the phased array can implement only piecewise constant phase shifts, the approximation to the ideal linear phase slope exhibits quantization errors [see Fig. 1(b)]. These phase errors cause higher-order grating lobes to be introduced into the output that lower the intensity of the central lobe and restrict the region over which it can be scanned unambiguously. For nonredundant scanning in one direction, the zero-order lobe can move only as far as the position of the undeflected first-order lobe. This defines the angular width of the useful scan zone to be $\Delta\theta_{\text{zone}} = (\lambda/d)$, where d is the basic modulator width. The useful scan-zone range is inversely proportional to the modulator size d, whereas the output spot size is inversely proportional to the full phased-array aperture of $D = Md$ (where M is the number of modulators in the array). It can be shown (see Ref. 4) that, under the Rayleigh resolution criterion, an M-channel phased array is capable of addressing M resolvable positions within the useful scan zone. Continuous scan-angle control is guaranteed if there is independent control of each modulator in the array (i.e., M control lines), but this becomes impractical and expensive as the number of modulators becomes large.

For modeling purposes consider a 1-D phased array with M pistonlike phase modulators that has a linear phase slope of $\alpha = \Delta\varphi/d$ programmed across the array [see Fig. 1(b)]. The array functions as an M-step echelon grating with a constant phase increment $\Delta\varphi$ and step width d. Its general transmission function

$T_0(x)$ can be described by an apertured sequence of increasing phase steps as

$$T_0(x) = W(x) * \sum_{m=0}^{M-1} \delta(x - md)\exp(im\Delta\varphi), \qquad (1)$$

where $W(x)$ is a windowing function of finite extent [$W(x) = 0$, for $|x| > d/2$], d is the modulator width, $\Delta\varphi$ is the phase increment between adjacent modulators, $m\Delta\phi$ is the phase value of the mth modulator, M is the number of modulators in the array, the asterisk denotes a convolution operation, and $\delta(x)$ is an idealized δ function. The windowing function $W(x)$ permits a generalized description of the phased array that can include partial fill-factor effects and other periodic aberrations. The far-field intensity pattern from such a phased-array deflector is proportional to the square of the Fourier transform of $T_0(x)$ and can be written in the form (see Ref. 2)

$$I^{\mathrm{OUT}}(\bar{\theta}) = C\,\mathrm{EF}(\bar{\theta})\mathrm{AF}(\bar{\theta} - \bar{\theta}_S), \qquad (2)$$

where C is a constant of proportionality and the element factor EF and the array factor AF are defined as

$$\mathrm{EF}(\bar{\theta}) \equiv |\mathcal{F}\{W(x)\}|^2, \qquad (3a)$$

$$\mathrm{AF}(\bar{\theta} - \bar{\theta}_S) = \left(\frac{\sin\left\{M\pi\left(\frac{d}{\lambda}\right)[\bar{\theta} - \bar{\theta}_S]\right\}}{M\sin\left\{\pi\left(\frac{d}{\lambda}\right)[\bar{\theta} - \bar{\theta}_S]\right\}} \right)^2, \qquad (3b)$$

respectively. Here $\mathcal{F}\{\cdots\}$ represents a Fourier transform operation, and the generalized angular parameters $\bar{\theta}$ and $\bar{\theta}_S$ are defined as

$$\bar{\theta} \equiv \sin(\theta) = \lambda\nu, \qquad (4a)$$

$$\bar{\theta} \equiv \sin(\theta_S) = \left(\frac{\Delta\varphi}{2\pi}\right)\left(\frac{\lambda}{d}\right). \qquad (4b)$$

The element factor EF (also known as the form factor) is defined as the Fourier transform of the windowing function, and it dictates the number of diffraction orders with relatively strong intensity. The array factor AF (also known as the interference term) represents the unattenuated diffraction spectra computed as the normalized Fourier transform of M infinitely narrow slits spaced a distance d apart. Plots of these factors are given in Fig. 2. The generalized angular coordinates in Eqs. (4) are designated with overbars and are equivalent to the sines of their respective angles. The parameter $\bar{\theta}$ [Eq. (4a)] is directly proportional to the spatial-frequency component ν of the object spectra; the translation parameter $\bar{\theta}_S$ [Eq. (4b)] is directly related to the programmed phase slope of $\alpha \equiv \Delta\varphi/d$ because $\alpha = (2\pi/\lambda)\sin(\theta_S)$. Under paraxial conditions the sine parameters in Eqs. (4a) and (4b) can be reduced to the simple angles θ and θ_S, respectively. Note that the form of Eq. (2) shows that the output intensity of a basic phased-array deflector consists of a *fixed* element-factor EF envelope and a *translatable* array-factor AF term. The spectra described by the AF term can be shifted arbitrarily by the programmable value $\bar{\theta}_S$.

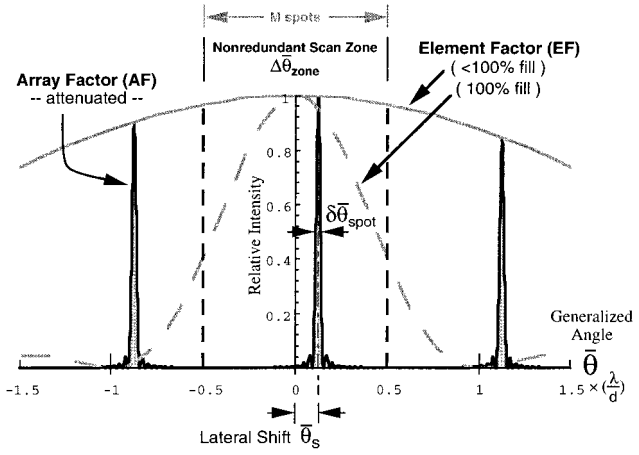

Fig. 2. Central lobes of the normalized far-field intensity pattern $I^{\mathrm{OUT}}(\theta)$ of a 1-D echelon grating deflector with $M = 32$ channels, a fill factor of $w/d = 1/5$ [solid envelope curve (EF)], and a deflection angle of $\bar{\theta}_S = (1/8)(\lambda/d)$. The ideal fill-factor envelope ($w/d = 1$) is shown as a dashed curve.

An analytic form for the element factor EF in Eq. (3a) can be given if a simple windowing function of the form $W(x) = \mathrm{rect}[x/w] = 1$ for $|x| \le w/2$ and $|x| = 0$ elsewhere is assumed. This windowing function represents a clear aperture of width $w \le d$ over each modulator. The element factor corresponding to this simple window is a sinc envelope of half-width $\Delta\bar{\theta}_{\mathrm{ENV}} = (\lambda/w)$ and can be written as

$$\mathrm{EF}(\bar{\theta}) = \left[\left(\frac{w}{d}\right)\mathrm{sinc}\left(\frac{\bar{\theta}}{\Delta\bar{\theta}_{\mathrm{ENV}}}\right)\right]^2, \qquad (5)$$

where $\mathrm{sinc}(\mu) \equiv \sin(\pi\mu)/(\pi\mu)$ and (w/d) represents the fill factor of the modulators. [Note that approximately (d/w) diffraction orders will pass into the output with relatively strong intensity.]

Many key features of a phased-array deflector can be explained with theoretical descriptions, which are summarized in Fig. 2. This figure plots the calculated output intensity of Eq. (2) by use of Eqs. (3b) and (5) and depicts three diffraction orders of the far-field intensity pattern from a 32-channel phased-array deflector with a fill factor of $w/d = 1/5$. Note that multiple spectra occur in the phased-array output whenever the fill factor is significantly less than 1. The spectra are shifted laterally by an amount $\bar{\theta}_S = (\Delta\varphi/2\pi)(\lambda/d)$, which can be arbitrarily set by a change in the phase-step increment $\Delta\varphi$. With continuous control of $\Delta\varphi$ over the phase range $[-\pi, \pi)$, the phased array can steer an incident monochromatic beam over a continuous range of angles within the nonredundant scan zone $|\bar{\theta}_S| < \frac{1}{2}(\lambda/d)$. This scan zone is determined by the region over which the central lobe can be steered unambiguously without encroaching on the $\pm$1st order lobe regions.

The output spectra have spot widths $\delta\bar{\theta}_{\mathrm{spot}}$ propor-

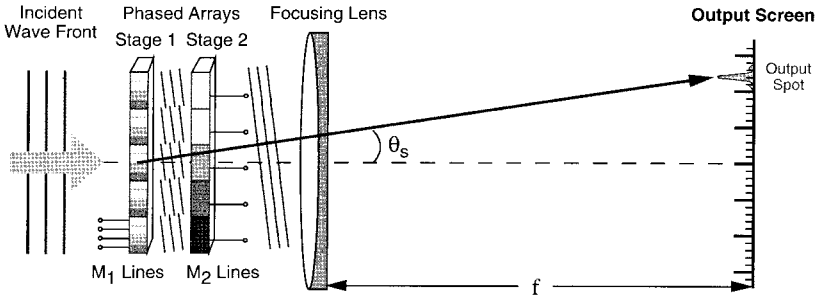

Fig. 3. Basic optical layout of a two-stage phased-array cascade with a reduced number of external connections. Stage 1 is addressed by M_1 control lines and stage 2 by M_2 control lines. By itself, stage 1 can deflect to only discrete output angles (shown as thick tick marks on the output screen).

tional to (λ/D). For an M-channel array there are M resolvable positions (by use of the Rayleigh criterion) that fall within the nonredundant scan zone. Because the intensity of the central lobe falls off with an increasing deflection angle (delimited by the element-factor envelope), one can further restrict the allowed scan zone to guarantee a specific minimum DE of $\eta \geq \eta_{MIN}$ for all scan points but at the cost of fewer than M resolvable scan positions. This is the same as restricting the amount of allowed phase quantization $\Delta\phi$. (See Appendix B for further discussion of the DE of phased-array deflectors.)

4. Cascading Concepts

Cascading is a useful strategy for achieving high switching complexity by use of a sequential array of simple switching elements. It can be applied to reduce the number of connections required to control a complex switching network. Beam deflectors fall into the category of optical switching elements, and arranging deflectors in a multistage cascade can greatly reduce the number of control lines needed to steer an optical beam, while still providing continuous, high-resolution scan control. In principle, a linear sequence of R deflector elements, each capable of addressing N spots, could address as many as R^N resolvable spots, if multiplicative resolution enhancement[16] is assumed. Several hardware-based cascading techniques have been investigated as a means of increasing the resolution of existing E-O deflectors.[17,18] Cascading has also been employed with hybrid deflector technologies to derive continuous deflection control from an inherently discontinuous beam-steering device.[19] Application of such cascading techniques to phased-array deflectors can achieve high-resolution scanning systems with a reduced number of control lines. However, as we show below, optimal performance is achieved by the choice of the proper cascading strategy and its implementation.

The fundamental principle behind a two-stage cascade is to set two deflectors with resolutions N_1 and N_2 in tandem and achieve a total scanner resolution of $N_R = N_1N_2$ points.[16] This is called a multiplicative cascade. We can realize such an arrangement by coupling a discrete-state deflector (stage 1) that is capable of addressing N_1 disjointed positions to a continuous-state deflector (stage 2) that is capable of steering to N_2 positions between each of the discrete states. By proper design of the two-stage combination, the discrete-state and the analog-state scanners can yield continuous scan-angle coverage of N_1N_2 resolvable output positions. Note that, for achieving the same far-field spot size from the coupled stages, both stages must possess the same device aperture. Phased arrays can be arranged in a multiplicative cascade, as shown in Fig. 3.

A. Aligned Two-Stage Phased-Array Cascade

In our experiments we used a particular cascade arrangement for the two-stage phased-array deflector in which both stages are aligned and a minimum number of control lines is required. (Throughout this paper, we refer to this specific geometry as an *aligned* two-stage phased-array cascade.) This configuration is shown schematically in Fig. 4 and lends itself well to theoretical modeling, as is detailed in Subsection 4.B. The first stage consists of a repeated sequence of small, identical phased-array deflectors $g(x)$, each containing M_1 modulators of width d_1. There are M_2 such subarrays in this stage that are all controlled by the same shared M_1 control lines. By itself, stage 1 is a discrete-state scanner. Stage 2 is a large phased array with M_2 channels—one channel per subarray in stage 1. (This is a minimum control-line count configuration.) Its broad modulators have a width of $d_2 = M_1d_1$, and they are aligned so as to overlap each of the subarrays in stage 1. Stage 2 requires M_2 independent control lines and functions as a continuous-state scanner. The two stages can be programmed independently with phase increments $\Delta\varphi_1$ and $\Delta\varphi_2$, respectively. Both arrays fill the aperture D, hence generating the same diffraction-limited angular spot size λ/D. But stage 1 can support deflection only to discrete angles of $\bar{\theta}_1(n) = n(\lambda/d2)$ (n is an integer), and only M_1 such angles fall within the useful scan zone of width λ/d_2. Stage 2 can address M_2 resolvable points over a narrow, continuous angular range of width λ/d_2. The deflection angles supported by the individual stages are summarized in Table 1.

The combination of the two stages can address

Table 1. Deflection Angles Supported by the Individual Stages of an Aligned Two-Stage Phased-Array Deflector[a]

Stage	Deflection Angle	Range	Scan Type
1	$\bar{\theta}_1(n) = (\lambda/d_2)$	n is the integer value	Discontinuous
2	$\bar{\theta}_2(r) = r(\lambda/d_2)$	$r \in [-1/2, +1/2)$	Continuous

[a]As shown in Fig. 4.

$N_R = M_1M_2$ resolvable points over the useful scan zone with just $M_1 + M_2$ control lines. This represents a logarithmic reduction in the number of control lines needed for full deflection control. For example, with two 32-channel phased-array stages ($M_1 = M_2 = 32$), one can build an $N_R = 1024$-point deflector that would require only 64 control lines instead of the 1024 lines that would be required by a single-stage deflector. Reducing the number of control lines becomes crucial at high array densities and when the electronic driver costs become prohibitive.

The concept of cascading optical phased-array deflectors to reduce the number of external connections was already proposed by McManamon *et al.*[1] Their concept used an architecture similar to that shown in Fig. 3 but without restricting the two stages to perfect alignment or aperture matching (i.e., $d_2 = M_1d_1$). Their technique employed a cascade-programming methodology that can be called a coarse–fine protocol. Patents on the implementation and programming of the coarse phased-array deflector of the form of stage 1 shown in Fig. 4 have been issued to authors of Ref. 1.

B. Two Programming Strategies

The coarse–fine protocol is the most direct method of controlling a two-stage deflector. However, as is shown theoretically in Section 5 and experimentally in Section 6, there exists an alternative strategy for programming an aligned phased-array cascade that can provide better optical performance with the same physical hardware. We call this second programming strategy a discrete–offset-bias protocol. Both protocols can use the same physical hardware but employ slightly different programming strategies. Before a more rigorous analysis, we now give a brief description of the two basic strategies that can be used to program an aligned two-stage phased-array cascade.

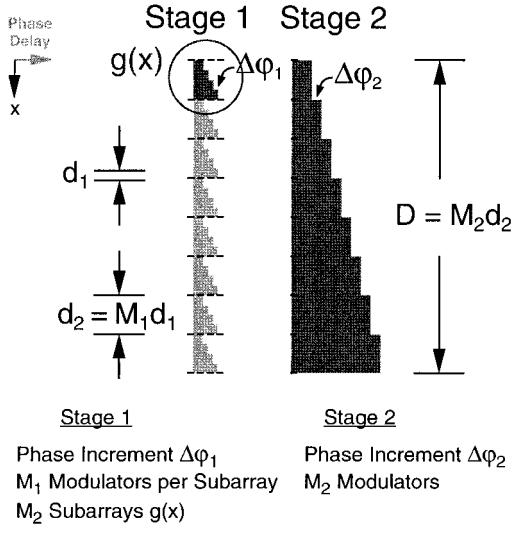

Fig. 4. Schematic layout of the unfolded phase distribution of an aligned two-stage phased-array cascade with a minimum control-line configuration.

1. *Coarse–Fine Programming Concept*

Under the coarse–fine protocol successive deflections of the incident beam are performed by the two stages to achieve pointing to the desired output position $\bar{\theta}_S$. Stage 1 is a discrete-state scanner that supports deflection to only discrete angles $\bar{\theta}_1(n) = n(\lambda/d_2)$ (n is an integer), shown as thick tick marks on the output screen illustrated in Fig. 3. These angles represent cases for which stage 1 is perfectly blazed, i.e., each subarray in stage 1 generates $n\lambda$ worth of optical path delay across its aperture. The second stage is then set to perform a slight angular correction by $\bar{\theta}_2 = \theta_S - \bar{\theta}_1$, which redirects the beam to the desired scan angle $\bar{\theta}_S$. In this way both stages simulate thin prisms with deflection angles $\bar{\theta}_1$ and $\bar{\theta}_2$, respectively, and *both* stages can therefore exhibit quantization errors [see Fig. 5(a)]. The multiplicative behavior of the phase errors from the two stages can lead to undesired noise lobes falling within the scan zone in the output and to a reduced intensity of the central peak. This is the protocol adopted in Ref. 1.

2. *Discrete–Offset-Bias Programming Concept*

The discrete–offset-bias protocol uses the same aligned-cascade hardware but employs a modified programming strategy that optimizes the optical performance of the two-stage deflector cascade. The philosophy here is to permit imperfect blazing from the first stage and correct any phase mismatches by use of constant phase shifts generated by the second stage. This concept was developed independently more than 20 years ago by Ninomiya[5,6] and Lee and Zook[7] as a scheme for resolution enhancement of E-O deflectors. Vasey *et al.*[10] employed it to reduce the number of control lines required in a channel-waveguide beam deflector. We employed this improved programming strategy to design a more efficient multistage phased-array deflector.

The discrete–offset-bias scheme for programming an aligned two-stage cascade is shown schematically by the deflected wave fronts depicted in Fig. 3. Under the discrete–offset-bias strategy, each of the small subarray deflectors in stage 1 is programmed to point the incident wave front directly to the desired scan direction $\bar{\theta}_S$, regardless of whether the discrete-state scanner (stage 1) can support that angle by itself. The subarrays in the first stage generate an array of tilted wave-front segments that are all directed toward $\bar{\theta}_S$, and these segments will interfere destructively if perfect blazing is not achieved (i.e., if $\bar{\theta}_S \neq n(\lambda/d_2)$, where n is an integer). Stage 2 is used

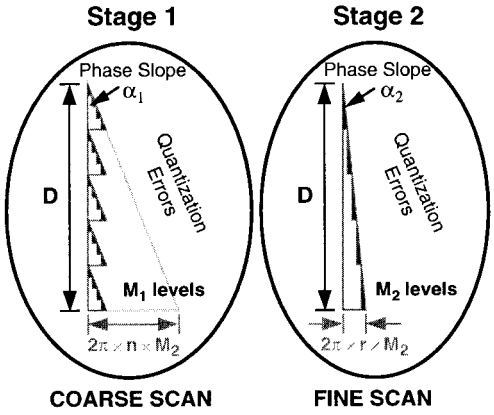

(a)

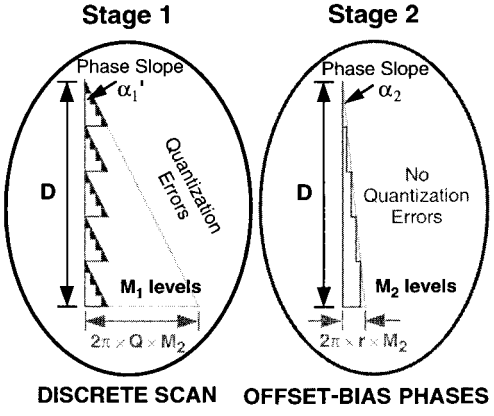

(b)

Fig. 5. Two basic strategies for programming an aligned two-stage phased-array deflector of the form given in Fig. 4. Equivalent phase profiles for the two stages are shown: (a) Coarse–fine programming; quantization errors occur in both stages. (b) Discrete–offset-bias programming; only stage 1 exhibits quantization errors.

to introduce constant phase offsets to the tilted wavefront segments passed by stage 1 so that, at the output of stage 2, all the tilted wave fronts are seamlessly joined. This guarantees maximum constructive interference into the far-field output angle $\bar{\theta}_S$. Note that stage 2 is also programmed for deflection to $\bar{\theta}_S$ in this scheme but is physically used only as a set of phase offsets. Because stage 2 just implements constant phase shifts, phase-quantization errors are found in only stage 1 [see Fig. 5(b)]. With this form of cascade programming the intensity of the central output lobe is maximized, and no spurious noise lobes will be generated within the scan zone. These qualitative statements are justified in quantitative terms in Section 5.

5. Aligned Two-Stage Phased-Array Theory

The far-field output from an aligned two-stage phased array can be derived by use of Eqs. (2) and (3) if we note that one can view the aligned two-stage cascade shown in Fig. 4 as a single-stage phased-array deflector (stage 2) that has a specialized windowing function $W_2(x) = g(x)$ (a subarray from stage 1). This type of analysis can be extended further to higher-order multistage arrangements. The windowing function $W_2(x)$ is itself a phased-array deflector with M_1 modulators of width d_1 and a programmed phase increment $\Delta\phi_1$. The windowing function $W_2(x)$ is applied to each modulator in stage 2, and it can be described analogously to Eq. (1) as

$$W_2(x) \equiv g(x) = W_1(x) * \sum_{m=0}^{M_1-1} \delta(x - md_1)\exp(im\Delta\varphi_1), \tag{6}$$

where $W_1(x)$ is the windowing function of the individual modulators in the first stage, the asterisk denotes a convolution operation, and $\delta(x)$ is an idealized δ function. According to Eq. (3a), the element factor for stage 2 EF_2 is equal to the square of the Fourier transform of its windowing function $W_2(x)$ given by Eq. (6). This calculation is identical to that used to convert the general phased array of Eq. (1) to its output given in Eq. (2). By applying Eqs. (2), (3b), and (5) to the phased array described by $W_2(x)$ in Eq. (6), we can write the stage 2 element factor EF_2 as

$$\mathrm{EF}_2(\bar{\theta}) = C'\mathrm{EF}_1(\bar{\theta})\mathrm{AF}_1(\bar{\theta} - \bar{\theta}_1), \tag{7a}$$

where

$$\mathrm{EF}_1(\bar{\theta}) = \left(\frac{w_1}{d_1}\right)^2 \mathrm{sinc}^2\left[\left(\frac{w_1}{\lambda}\right)\bar{\theta}\right], \tag{7b}$$

$$\mathrm{AF}_1(\bar{\theta} - \bar{\theta}_1) = \left(\frac{\sin\left\{M_1\pi\left(\frac{d_1}{\lambda}\right)[\bar{\theta} - \bar{\theta}_1]\right\}}{M_1 \sin\left\{\pi\left(\frac{d_1}{\lambda}\right)[\bar{\theta} - \bar{\theta}_1]\right\}}\right)^2, \tag{7c}$$

where C' is a constant of proportionality and EF_1 and AF_1 are the element factor and the array factor, respectively, of the stage 1 subarray $g(x)$. In Eqs. (7), w_1 and d_1 are the clear aperture and the full width of the modulators in stage 1, respectively, M_1 is the number of modulators per subarray in stage 1, and $\bar{\theta}_1$ is the programmed deflection angle of the first stage. As derived from Eq. (4b), this angle is defined as $\bar{\theta}_1 \equiv \sin(\theta_1) = (\Delta\varphi_1/2\pi)(\lambda/d_1)$, where $\Delta\varphi_1$ is the phase increment programmed onto the subarrays of stage 1. Equations (7) show that the stage 2 element factor EF_2 represents a multispiked envelope term of the form plotted in Fig. 2 but with broadened spikes of width (λ/d_2) that are laterally translated by $\bar{\theta}_1$.

The far-field intensity pattern $I_2{}^{\mathrm{OUT}}$ from the full two-stage phased-array cascade is obtained by application of Eqs. (2) and (3) to the stage 2 phased array and by use of Eqs. (7) as the element factor for this array. The result can be written in the form

$$I_2{}^{\mathrm{OUT}}(\bar{\theta}) = C\,\mathrm{EF}_1(\bar{\theta})\mathrm{AF}_1(\bar{\theta} - \bar{\theta}_1)\mathrm{AF}_2(\bar{\theta} - \bar{\theta}_2), \tag{8a}$$

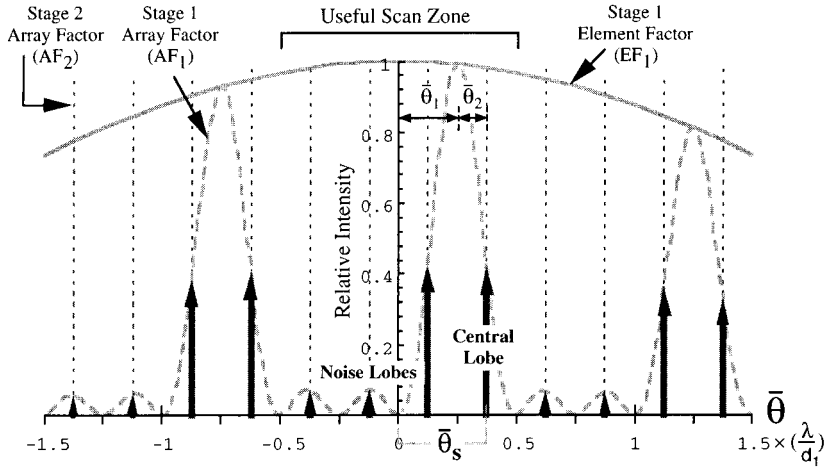

(a)

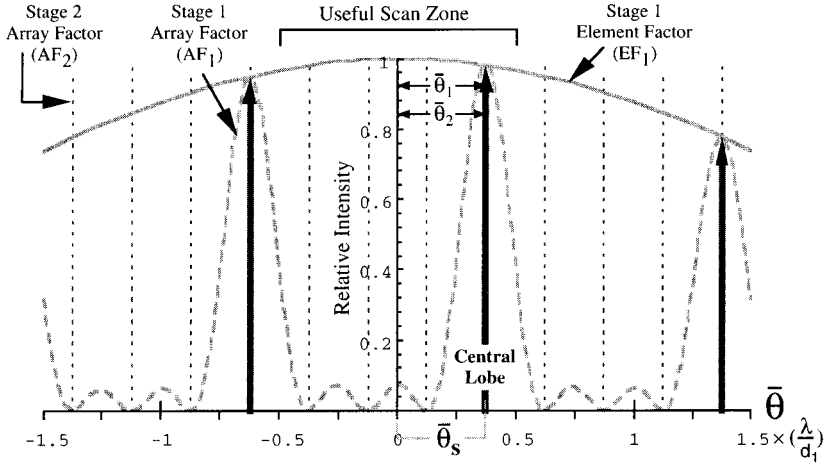

(b)

Fig. 6. Theoretical far-field intensity pattern I^{OUT} from an aligned two-stage phased-array cascade with a minimum control-line configuration. The cascaded arrays are programmed for deflection to $\bar{\theta}_S = (3/8)(\lambda/d_1)$ by use of (a) coarse–fine programming ($\bar{\theta}_S = \bar{\theta}_1 + \bar{\theta}_2$) and (b) discrete–offset-bias programming ($\bar{\theta}_S = \bar{\theta}_1 = \bar{\theta}_2$). There are $M_1 = 4$ modulators/subarray in stage 1; the fill factor is $w_1/d_1 = 1/5$.

where EF_1 and AF_1 are defined above in Eqs. (7b) and (7c), respectively, and

$$\mathrm{AF}_2(\bar{\theta} - \bar{\theta}_2) = \left(\frac{\sin\left\{ M_2 \pi \left(\frac{d_2}{\lambda} \right) [\bar{\theta} - \bar{\theta}_2] \right\}}{M_2 \sin\left\{ \pi \left(\frac{d_2}{\lambda} \right) [\bar{\theta} - \bar{\theta}_2] \right\}} \right)^2 . \quad (8b)$$

where AF_2 is the array factor for stage 2 and d_2, M_2, and $\bar{\theta}_2$ in Eq. (8b) are the modulator width, the total number of modulators, and the programmed deflection angle for stage 2, respectively. Note that $\bar{\theta}_2$ is defined by Eq. (4b) as $\bar{\theta}_2 \equiv \sin(\theta_2) = (\Delta\varphi_2/2\pi)(\lambda/d_2)$, where $\Delta\varphi_2$ is the phase increment programmed into stage 2. The spectra defined by the stage 2 array factor in Eq. (8b) have narrow spot widths proportional to $(1/M_2)(\lambda/d_2)$ and are translated laterally by $\bar{\theta}_2$.

From Eq. (8a) we see that the far-field intensity pattern from an aligned two-stage phased-array deflector consists of a global *fixed* envelope (EF_1), a *translatable* array-factor envelope (AF_1), and *translatable* diffraction spectra defined by AF_2. These terms are plotted in Fig. 6. The useful scan zone for the two-stage deflector is limited to a width of $\Delta\bar{\theta}_{\mathrm{zone}} = (\lambda/d_1)$, defined as the useful scan zone of a single subarray deflector $g(x)$ in stage 1. The output spectra have an angular width proportional to (λ/D), where $D = M_2 d_2 = M_1 M_2 d_1$ is the full device aperture. Note that the two array-factor terms, AF_1 and AF_2 [Eqs. (7c) and (8b)], can be translated independently by the angles $\bar{\theta}_1$ and $\bar{\theta}_2$, which are functions of the programmed phase increments $\Delta\varphi_1$ and $\Delta\varphi_2$, respectively. The two fundamental protocols for programming cascaded phased arrays differ in the way they select the translation angles $\bar{\theta}_1$ and $\bar{\theta}_2$. Below

we clarify the differences between the two programming strategies by examining a specific deflection example.

A. Aligned Two-Stage Cascade Example

Consider an aligned two-stage phased-array deflector of the form shown in Fig. 4 with $M_1 = 4$ modulators per subarray in stage 1, a fill factor of $w_1/d_1 = 1/5$, and an arbitrarily large number of subarrays ($M_2 \gg 1$). (Stage 2 modulators are assumed to be 100% filled with one modulator per subarray in stage 1.) The deflector is illuminated by a monochromatic beam of wavelength λ. The nonredundant scan zone of this deflector has an angular width of $\Delta\bar{\theta}_{\text{zone}} = (\lambda/d_1)$, where d_1 is the width of a phase shifter in stage 1, and for simplicity this zone is assumed to be centered about the optical axis. Figure 6 shows the ideal theoretical output from such a two-stage phased-array deflector that has been programmed for deflection to $\bar{\theta}_S = \frac{3}{8}(\lambda/d_1)$ by use of the coarse–fine protocol [Fig. 6(a)] and the discrete–offset-bias protocol [Fig. 6(b)]. Note that the output spectra defined by the stage 2 array factor AF_2 are plotted as narrow δ functions for simplicity. The actual spectra will have finite angular spot widths proportional to (λ/D), where $D = (M_1M_2)d_1$ is the full device aperture.

1. *Coarse–Fine Programming for* $\bar{\theta}_S = \frac{3}{8}(\lambda/d_1)$

The calculated output of the aligned two-stage deflector programmed with the coarse–fine protocol is shown in Fig. 6(a). Here stage 1 is programmed to deflect the incident beam to one of its allowed deflection angles $n(\lambda/d_2)$, choosing the specific angle $\bar{\theta}_1(n)$ that lies closest to $\bar{\theta}_S$. For this example we choose the $n = 1$ direction, giving $\bar{\theta}_1 = (\lambda/d_2) = \frac{1}{4}(\lambda/d_1)$, where $d_2 = 4d_1$ for the specified deflector arrangement. Stage 2 must provide an additional deflection by $\bar{\theta}_2 = \frac{1}{8}(\lambda/d_1)$ so that the total angular deflection is $\bar{\theta}_S = \bar{\theta}_1 + \bar{\theta}_2 = \frac{3}{8}(\lambda/d_1)$.

The coarse–fine programming translates stage 1's array-factor envelope AF_1 to the designated angle $\bar{\theta}_1$. The output spectra described by AF_2 (dashed vertical lines in Fig. 6) are translated by $\bar{\theta}_2$ so that one of the diffraction lobes will lie at the desired deflection angle $\bar{\theta}_S$. Because the two translatable terms AF_1 and AF_2 are not coaligned, the central output lobe at $\bar{\theta}_S$ has low intensity, and several noise lobes appear with strong intensity within the useful scan zone [see Fig. 6(a)]. Note that the deflection angle of $\bar{\theta}_S = \frac{3}{8}(\lambda/d_1)$ represents a worst-case situation for the coarse–fine protocol here, as it requires stage 2 to exhibit maximum quantization noise. A higher overall spot DE could be achieved if the number of phase shifters in the fine deflector (stage 2) were increased, but this would require greater system complexity than the minimum configuration modeled in Fig. 6(a). (Further details are given in Appendix B.)

2. *Discrete–Offset-Bias Programming for* $\bar{\theta}_S = \frac{3}{8}(\lambda/d_1)$

Optimal use of the incident light energy is achieved by means of programming the deflector cascade with the discrete–offset-bias protocol. Figure 6(b) shows the expected output for this case. Here both stages are programmed for deflection directly to $\bar{\theta}_S$, i.e., $\bar{\theta}_1 = \bar{\theta}_2 = \bar{\theta}_S = \frac{3}{8}(\lambda/d_1)$. In this way the peaks of both the translatable terms—the envelope term AF_1 and the output spectra AF_2—are coaligned directly above the desired deflection angle $\bar{\theta}_S$. Only one strong diffraction order appears within the nonredundant scan zone of the output because the other spectral orders within this zone fall near the zeroes of the stage 1 array-factor envelope AF_1 [see Fig. 6(b)]. The strong central lobe has a maximum intensity that is limited solely by the fixed stage 1 element-factor envelope EF_1. Note that, under the discrete–offset-bias protocol, the combination of stages 1 and 2 of the phased-array cascade work in unison to emulate a large single-stage array deflector programmed for deflection to $\bar{\theta}_S$. And unlike with the coarse–fine protocol, no quantization errors occur in stage 2 because it is responsible for only flat phase offsets.

B. Discussion of the Cascading Theory

Analysis of the theoretical output as a function of the deflection angle θ_S shows fundamental differences between the two cascade-programming techniques. Under the coarse–fine protocol the output exhibits discontinuous jumps in the central lobe intensity as a function of scan angle because stage 1 operates in a discontinuous fashion as the scan angle is increased. This protocol also generates noise lobes in the output that become most severe when there is maximum misalignment between the array-factor terms AF_1 and AF_2 [as shown in Fig. 6(a)]. These effects are artifacts of the large quantization errors occuring in stage 2 when the chosen deflection angle θ_S cannot be addressed by stage 1 alone, and they can be alleviated in part by an increase in the number of modulators in the fine stage (stage 2) to reduce its phase-quantization errors.

Alternatively, the discrete–offset-bias protocol achieves an optimal DE that is a monotonically decreasing function of the deflection angle bracketed solely by the fixed element-factor envelope EF_1. Under this second protocol all the residual phase errors occur in only stage 1, and the intensity of the central lobe is guaranteed to be maximum for all angles. (Appendix B gives specific formulas for the DE's of the two protocols and quantitatively demonstrates the effects described above.) Note that this comparative analysis is strictly valid for only an *aligned* two-stage cascade of the form shown in Fig. 4.

If alignment between the stages cannot be guaranteed because of physical or hardware constraints, the coarse–fine protocol must be used. In this case both stages function as independent single-stage phased-array deflectors. If we assume completely filled modulators, the ideal DE of each stage can be derived from Eqs. (4b) and (5) and written as $\eta_i(\Delta\varphi_i) = \text{sinc}^2[\Delta\varphi_i/2\pi]$, where η_i and $\Delta\varphi_i$ are the DE and the phase increment of the ith stage, respectively. (A slightly more general treatment can be found in Appendix B.) Low-noise lobes and a minimum total

DE η_{MIN} can still be achieved by oversampling of the linear phase profiles of the two stages so that $\eta_{TOT} \equiv \eta_1\eta_2 \geq \eta_{MIN}$, is satisfied for all deflection angles. This is equivalent to increasing the number of modulators in both stages (i.e., increasing M_1 and M_2) and restricting the maximum allowed phase increments of the two stages, $|\Delta\varphi_1|^{MAX}$ and $|\Delta\varphi_2|^{MAX}$, to be less than π. This is the approach employed by the coarse–fine phased-array deflector described in Ref. 1. Such an approach inherently requires more than $M_1 + M_2$ control lines to achieve a deflector resolution of $N_R = M_1M_2$ points and therefore needs a larger phased-array architecture than an aligned two-stage cascade programmed with the discrete–offset-bias protocol, which would require only $M_1 + M_2$ control lines.

The theoretical considerations show that an aligned-cascade arrangement programmed with the discrete–offset-bias protocol is the preferred cascade arrangement and makes the most efficient use of the existing modulators. It achieves the highest overall DE for the least number of control lines. We devised a novel compact design for an aligned two-stage phased-array cascade in which both stages are integrated onto a single PLZT wafer.[20] Similar compact implementations can be made with other optical phased-array technologies such as liquid-crystal-based phased arrays.

6. Experimental Results

A. Lanthanum-Modified Lead Zirconate Titanate–Based Optical Phased Array

To demonstrate the operation of a cascaded phased-array deflector, we employed a pair of 32-channel optical phased arrays fabricated by using PLZT. PLZT is a transparent ferroelectric ceramic exhibiting strong E-O effects.[21] We chose to use PLZT 9.0/65/35 for phase modulation because of its large quadratic E-O coefficient, broadband optical transmission range, fast switching response, and good thermal stability. It can be used at wavelengths in the visible through the mid-IR spectral ranges and can provide very fast switching rates (faster than 1 μs). Our group previously demonstrated phased-array beam deflection with PLZT in a single-stage arrangement.[12] We call this type of device PAGES (phased-array grating electro-optic scanner).

Figure 7 shows a fabricated 32-channel phased array based on PLZT 9.0/65/35 and mounted in a gold-plated package. This PLZT composition offers a very strong quadratic E-O coefficient (3.8×10^{-16} m^2/V^2) with minimal residual linear effects. We fabricated the electrodes on one surface of a 350-μm-thick PLZT wafer by using vacuum-evaporated chrome gold, standard photolithographic techniques, and wet etching. The raw device was then mounted into a 0.75-in. (1.91-cm) square flat-pack package with an open aperture cut through the base plate so that it could be used in transmission mode. The active window of the device measures 12.8 mm × 10.0 mm. Each modulator has a dual-aperture configuration consisting of a central source electrode 160 μm wide surrounded by two 160-μm-wide ground electrodes that provide electrical isolation between the modulators. The modulator grating period is d = 400 μm, and the interelectrode gaps (clear apertures) are w = 40 μm, yielding an effective fill factor of $w/d = 1/10$. Voltage supplied to a specific modulator induces fringing electric fields within the substrate that cause a symmetric index change in both apertures of that modulator. The strongest modulation occurs for light polarized perpendicular to the electrodes. This device is a single-stage 1-D optical phased array with independent control lines for each of the modulators. One can also build a two-dimensional deflector by crossing a pair of these transverse 1-D arrays with a λ/2 plate oriented at 45° sandwiched between the devices.

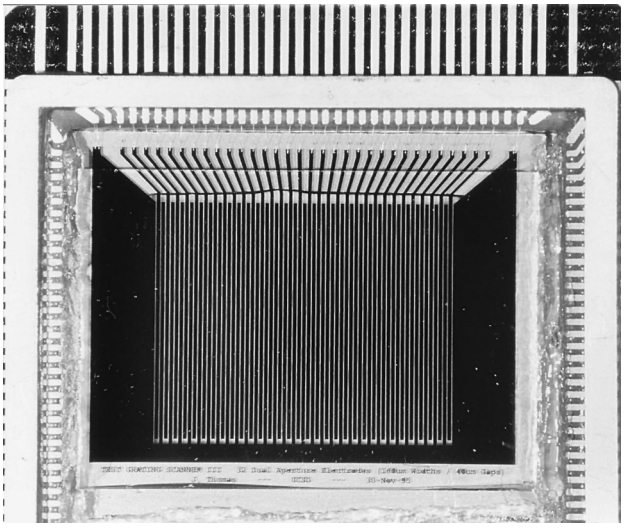

Fig. 7. Packaged 32-channel optical phased array made with PLZT. The active window has dimensions of 12.8 mm × 10.0 mm.

The phase response of the modulators was measured by use of a modified Young's double-slit experiment in which one of the two slits is active (with a positive applied voltage) and the other slit is grounded. The relative phase shift of the active slit is determined by measurement of the lateral shift of the fringes in the far-field interference pattern.[22] The measured average phase-modulation response of the PLZT modulators illuminated by a collimated He–Ne beam (λ = 633 nm) polarized perpendicular to the electrodes is shown in Fig. 8. The modulation curve follows the expected quadratic E-O behavior up to 150 V and then flattens out as a result of saturation effects in the PLZT. The measured full-wave voltage ($V_{2\pi}$) of these modulators was 318 V. As is required for a fully programmable phased-array device, this modulator design provides continuous phase control over the range [0, 2π) for the given He–Ne wavelength. Note that lower full-wave voltages can be realized by use of alternative electrode structures like buried electrodes, but simple surface electrodes were used here for the basic demonstration of a phased-array cascade.

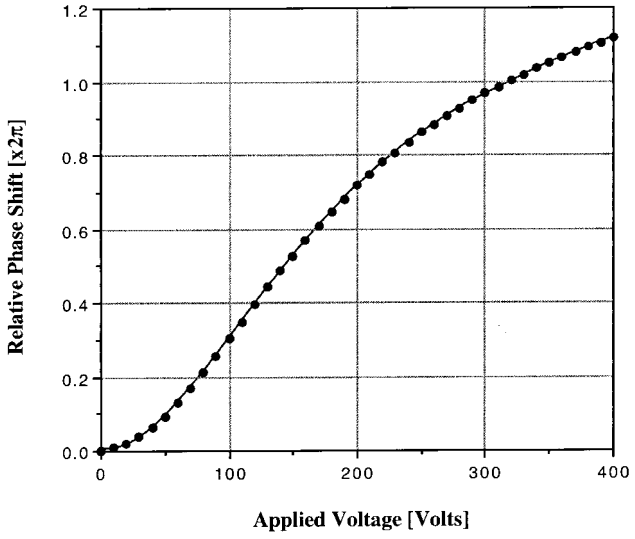

Fig. 8. Average measured phase-modulation response of the PLZT modulators in the 32-channel phased-array device shown in Fig. 7.

B. Cascade Experiments

We implemented an aligned two-stage cascade by mounting a pair of 32-channel test devices back to back so that the clear gaps from the first array were aligned directly over the respective gaps in the second array. In the actual mounting the two PLZT wafers representing the individual phased-array stages were separated by 1.5 mm with their electrode surfaces facing outwards.

The control lines of the two devices were externally interconnected to simulate the cascade arrangement of Fig. 4. Specifically, for the stage 1 device, the control lines were interconnected to form a series of $M_2 = 8$ subarrays containing $M_1 = 4$ modulators each. The modulators in corresponding positions in each of the subarrays were then connected in parallel. In this way stage 1 becomes a discrete-state scanner controlled by just four control voltages applied in distributed fashion to each of the subarrays. (This implementation of a coarse array from a large array of independent phase modulators is similar to that described by Dorschner and Resler[11] for a liquid-crystal-based optical phased array.)

The control lines of the stage 2 device were connected together to form a series of eight subarrays with four neighboring modulators grouped into each subarray. Here the control lines for each subarray were electrically ganged together. Thus stage 2 was addressed with eight control voltages, one voltage for each subarray. The two-stage phased-array device is fully addressed by just $M_{\mathrm{TOT}} = M_1 + M_2 = 12$ control voltages and is capable of addressing $N_R = 32$ resolvable positions. Note that a single-stage device with an equivalent resolution would require 32 independent control voltages. A scanning experiment was performed with the two-stage device to examine the deflector output at each of the 32 fundamentally resolvable output positions. An array of 12 potentiometer-controlled voltage dividers was used to provide static programming for the two stages. For each of the output positions the cascade was programmed by use of both the course–fine protocol and the discrete–offset-bias protocol, and the outputs were compared. An expanded and collimated He–Ne laser beam polarized perpendicular to the electrodes was used to illuminate the active window of the coupled phased arrays. A Fourier transform lens ($f = 375$ mm) was placed behind the phased arrays to produce output spectra at the back focal plane of the lens. These spectra were imaged onto a CCD array with a 6× microscope objective. For eliminating any undesired additional cosinusoidal envelope over the diffraction orders, which is due to the dual-aperture transmittance of the modulators, a horizontal masking arrangement was employed so that only a single gap from each modulator received illumination. In the vertical direction a 2-mm-wide slit mask was used across the active window of the devices to reduce aberrations from the nonplanarity of the PLZT substrates. The angular width of the nonredundant scan zone (λ/d_1) was roughly 0.1° for this test device, which guarantees that all the experimental outputs lie well within the paraxial regime.

Figure 9 shows the recorded output of the two-stage deflector for all rightward-shifted resolvable deflection angles $\theta_S = (j/32)(\lambda/d_1)$, whereas $j = 0, \ldots, 16$. [The sequence of leftward-deflected beams (where $j = -15, \ldots, -1$) have the same appearance as those shown in Fig. 10 but are reflected symmetrically about the optical axis.] The topmost image in both columns shows the output spectra when the deflectors are turned off. Several diffraction orders are apparent in the output because of the low effective fill factor (1/10) of the modulators. Only the three central diffraction orders (0th and ±1st orders) are shown in Fig. 9. The optical axis is delineated by the central-order spot in the topmost images, and the primary nonredundant scan zone is centered about this spot with a width equal to the spacing between diffraction orders, i.e., $(\lambda/d_1) = 0.1°$. For each image the intensity of the laser beam was adjusted to allow bright imaging of the central order without influencing the spatial distribution or the relative intensity of the output lobes. Figure 10 shows plots of the absolute intensity of the CCD data for the case of $\theta_S = (4/32)(\lambda/d_1)$.

The two stages were programmed by use of both the coarse–fine protocol [Fig. 9(a)] and the discrete–offset-bias protocol [Fig. 9(b)] in the manner detailed in Appendix A. All phase shifts were reduced by modulo 2π to the range $[0, 2\pi)$ in the actual programming. The output images in Fig. 9 clearly show progressive lateral deflection of the far-field spectra under both programming strategies. The discrete–offset-bias protocol displays good contrast of the shifted central lobe at all deflection angles. The coarse–fine protocol shows strong noise lobes in its output at several deflection angles. The positions $\theta_S = (j/32)(\lambda/d_1)$, with $j = -8, 0, 8, 16$, correspond to the discrete states addressable by stage 1 alone. At

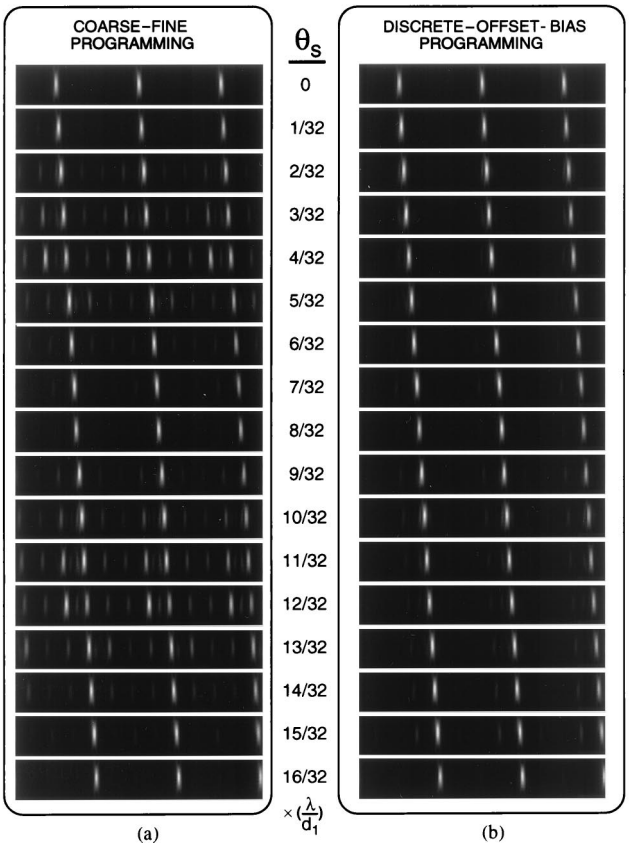

Fig. 9. One-dimensional beam-steering output by use of two 32-channel PLZT phased arrays in an aligned two-stage cascade with $M_1 = 4$ and $M_2 = 8$. The cascaded arrays were programmed for deflection to various angles θ_S by use of (a) the coarse–fine protocol and (b) the discrete–offset-bias protocol. Only half of the 32 resolvable scan outputs are shown.

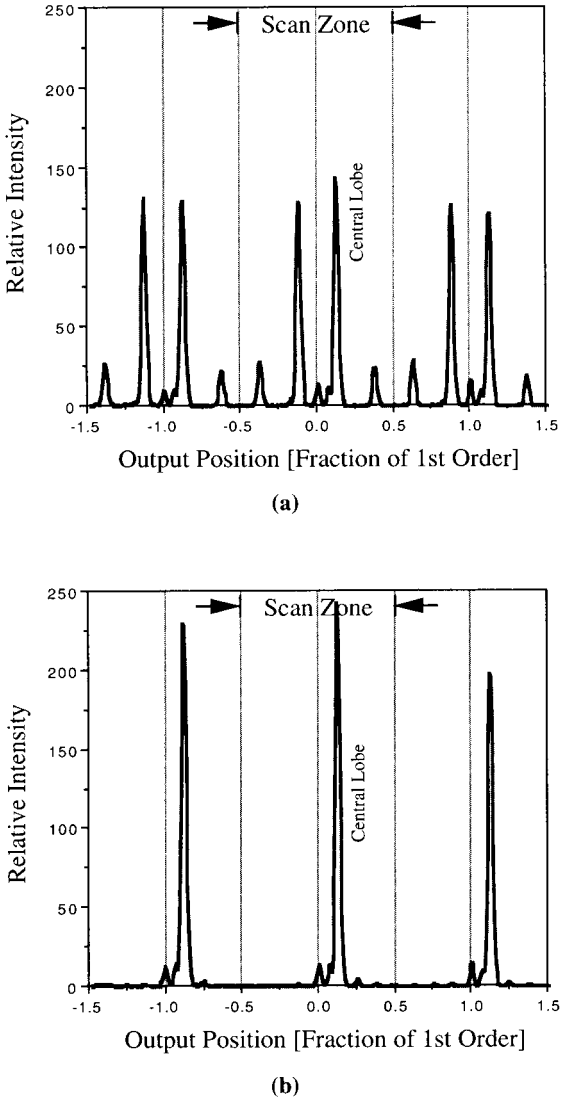

Fig. 10. Horizontal traces through the CCD data shown in Fig. 9 for a deflection angle of $\theta_S = j/32)(\lambda/d_1)$. Strong secondary noise lobes appear in the scan zone under coarse–fine programming.

these positions both protocols generate the same programmed phase values for the two stages; hence they exhibit identical output spectra. Under the coarse–fine protocol noise lobes become quite prominent within the scan pattern at angles at which stage 2 must perform strong deflection (i.e., where $j = -12$, -4, 4, 12).

The scan profiles shown in Fig. 10 show that the additional lobes appearing in the coarse–fine output reduce the absolute intensity of the primary scan peak. Small noise lobes also appear at large deflection angles under discrete–offset-bias programming, and these can be attributed to partial amplitude losses in the PLZT modulators at high voltages. Measurements of the primary scan peak intensity versus the deflection angle coincide well with theoretical predictions for the DE's of the two protocols (as outlined in Appendix B). Overall the discrete–offset-bias protocol produced higher peak intensities with only minimal noise lobes, which can be attributed to scattering losses in the modulators at high drive voltages.

Full scan-zone coverage was achieved with the two-stage cascade, as shown in Fig. 11. Traces of alternating Rayleigh beam positions are shown, which fill the nonredundant scan zone delineated by $|\theta_S| \leq (1/2)(\lambda/d_1)$. The scan-zone width extended over 129 pixels on the CCD camera in our measurements. The average spot width (full width at half-maximum) of the output points was found to be 5.1 pixels, roughly 25% larger than the expected diffraction-limited width of $129/32 = 4.0$ pixels. This spot broadening is primarily due to phase distortions among modulators and aberrations in the optical setup. In a final set of experiments, we programmed the two-stage device for deflection to angles of $\theta_S = (1/64)(\lambda/d_1)$, $(1/\pi)(\lambda/d_1)$ to demonstrate continuous beam-position control. Accurate subspot size-positioning control was confirmed. The two-stage phased-array deflector with a reduced number of control lines is capable of continuous deflection-angle control.

7. Conclusions

An optimal arrangement for cascading 1-D phased-array deflectors has been presented. Cascading is

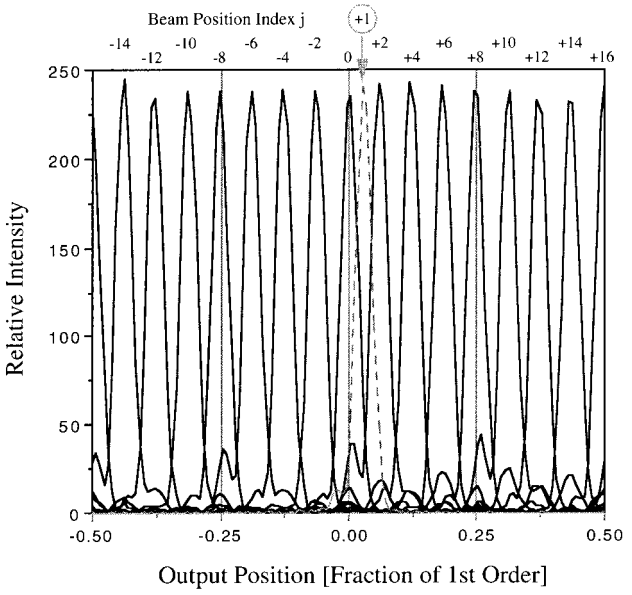

Fig. 11. Intensity profiles of the two-stage deflector output for the primary deflection angles of $\theta_S = j/32(\lambda/d_1), j = -14, \ldots, +16$ (solid curves) and $j = +1$ (dashed curve) under discrete–offset-bias programming. The data cover the central nonredundant scan zone in the output.

required by high-resolution scanning systems to reduce the number of control lines significantly and can be achieved with phased arrays while still allowing for continuous deflection-angle control, restricted voltage requirements ($V_{\text{applied}} \leq V_{2\pi}$), and compensation for nonideal E-O behavior and aging effects. Both theoretical and experimental results have shown that an aligned multistage phased-array cascade programmed by use of the discrete–offset-bias strategy can offer superior optical performance compared with the same minimum configuration programmed with the coarse–fine strategy. The aligned-cascade arrangement provides multiplicative resolution enhancement, and the number of control lines required for a deflector of resolution N_R can be reduced to the order of $2\sqrt{N_R}$.

The theoretical analysis introduced here employed a Fourier based examination of the aligned two-stage phased-array deflector and exploited the fact that the subarrays in the first stage could be considered as windowing functions for the second stage. Both stages generate array-factor terms that can be shifted independently, depending on the phase ramps programmed into the respective stages. The maximum DE for the central peak is obtained when both array-factor terms are lined up over the desired output angle θ_S (as with discrete–offset-bias programming) and when all modulators are 100% filled. The recursive Fourier analysis can be applied directly to higher-order, aligned, multistage arrangements with the consistent result that optimal performance is achieved when all translatable array-factor terms are lined up over the output angle. Higher-order cascades would require even fewer control lines than a two-stage cascade for the same overall deflector resolution N_R.

Two 32-channel optical phased arrays based on PLZT were fabricated and used to demonstrate the cascading concept experimentally and to show the improved performance of the discrete–offset-bias programming strategy. The experimental two-stage device was able to address all 32 resolvable beam positions with just 12 control lines. It was further capable of continuous beam steering to any angle between these beam positions. Proof-of-concept demonstrations were made with the current PLZT arrays, which have a low fill factor of 1/10 as a result of the broad surface electrodes on the substrates. Alternative electrode designs and the inclusion of lenslet arrays on both sides of the present devices would enhance the effective fill factor and generate a higher overall DE for the central peak. The present experiments, however, verify that the two-stage phased-array deflector can provide precise and continuous deflection-angle control with a reduced number of control lines.

The multistaging technique is a practical means for simplifying phased-array deflector control without compromising its beam-steering flexibility. The best performance is achieved with the least number of control lines by use of an aligned phased-array arrangement and by programming of the stages with the discrete–offset-bias strategy. Such phased-array cascading techniques are very useful and could be applied to all forms of space-fed phased-array systems, including ultrasonic and microwave-based phased arrays.

Appendix A: Phased-Array Programming Formulas

1. Single-Stage Beam Deflection

To deflect an incident monochromatic beam by an angle θ_S, it is necessary to program a phased array with an appropriate fixed phase increment $\Delta\varphi$ between each phase shifter in the array. By means of Eq. (4b), the required phase-step increment $\Delta\varphi$ (in radians) is given by

$$\Delta\varphi = 2\pi\left(\frac{\lambda}{d}\right)\sin(\theta_S), \tag{A1}$$

where λ is the wavelength of the incident beam, d is the modulator spacing, and θ_S is the desired deflection angle. The phase-step increment is a fundamental parameter and dictates how the entire array should be programmed. After $\Delta\varphi$ is determined, the phase shifts of the modulators in an M-channel phased array can be set as $\varphi_m = m\Delta\varphi + \varphi_{\text{AVE}}$ for $m = 0, \ldots, M-1$, where φ_m is the absolute phase shift of the mth modulator and φ_{AVE} is an arbitrary constant phase value. For monochromatic cw illumination, as is assumed here, all phase shifts can be reduced by modulo 2π without a functional change in the operation of the phased array. This helps to limit the amount of physical phase shift that must be produced by any modulator to the range $[0, 2\pi)$. In all our

experiments the actual phase shifts programmed into the modulators were *reduced* phase shifts. For deflection by an angle θ_S, the phased array is programmed with reduced phase shifts $\hat{\varphi}_m$, given by

$$\hat{\varphi}_m \equiv [\varphi_m] \bmod 2\pi$$
$$= [m\Delta\varphi + \varphi_{\mathrm{AVE}}] \bmod 2\pi, \quad m = 0, \ldots, M-1. \quad \text{(A2)}$$

Here $\hat{\varphi}_m$ is the reduced phase shift of the mth modulator, $\Delta\varphi$ is the phase increment determined by Eq. (A1), φ_{AVE} is an arbitrary constant (typically set to 0), and M is the number of modulators in the phased array. The programming of the phased array is completed by conversion of the reduced phase shifts from Eq. (A2) to corresponding control voltages and then application of these voltages to their respective modulators. The phase-modulation transfer curve (Fig. 8) defines the conversion between phase shift and control voltage for the PLZT phase modulators used in our experiments. Note that using reduced phase shifts guarantees that all the applied voltages will be less than a full-wave voltage ($V_{2\pi}$) of the modulators.

2. Two-Stage Beam Deflection

In the two-stage implementation of phased-array beam steering the individual stages are programmed with separate phase increments $\Delta\varphi_1$ and $\Delta\varphi_2$, which are functions of their individual deflection angles θ_1 and θ_2, respectively, and their modulator spacings d_1 and d_2, respectively. The values for the individual deflection angles are dictated by the overall deflection angle θ_S, as outlined in Subsection 4.B, and they are dependent on the type of cascade and the choice of programming protocol.

We now derive the operational programming formulas used to set the phases in an aligned two-stage phased-array deflector by following either the coarse–fine protocol or the discrete–offset-bias protocol. The aligned-cascade layout is a minimum control-line configuration of the form shown in Fig. 4 in which stage 1 is the coarse (or discrete) stage and stage 2 is the fine (or offset-bias) stage.

Consider establishing beam deflection by an arbitrary generalized angle $\bar{\theta}_S = Q(\lambda/d_2)$, where $\bar{\theta}_S \equiv \sin(\theta_S)$, λ is the beam wavelength, d_2 is the modulator spacing in stage 2, and Q is an arbitrary real-valued multiplicative constant. Q must be restricted to the range $|Q| \le M_1/2$ to keep the central output spot within the nonredundant scan zone. Here (λ/d_2) represents the angular spacing between the discrete states (i.e., blazed orders) that can be addressed directly by stage 1 alone, and M_1 is the number of modulators per subarray in stage 1. The constant Q can conveniently be decomposed into an integer part n and a fractional part r such that $Q = n + r$ and the full deflection angle can be redefined as

$$\bar{\theta}_S = Q\left(\frac{\lambda}{d_2}\right) = (n + r)\left(\frac{\lambda}{d_2}\right), \quad \text{(A3)}$$

where $n \equiv \mathrm{round}[Q]$ selects the integer value closest to Q and $r \equiv Q - n$. The parameter r is real valued and is guaranteed to lie in the range $[-0.5, 0.5)$ by this definition. With this decomposition the deflection angles required by each phased-array stage in the cascaded deflector can readily be determined.

A. *Coarse–Fine Programming of an Aligned Cascade*

Under the coarse–fine protocol the first stage is programmed to deflect the incident beam by an angle $\bar{\theta}_1 = n(\lambda/d_2)$ and the second stage by an angle $\bar{\theta}_2 = r(\lambda/d_2)$. The angle $\bar{\theta}_1$ represents the nth blazed diffraction order for the coarse deflector (stage 1). Each subarray in stage 1 functions as an M_1-channel phased-array deflector with beam steering to $\bar{\theta}_1$. Stage 2 acts as a single M_2-channel phased-array deflector with beam steering to $\bar{\theta}_2$. If we note that $d_2 = M_1 d_1$ (for a minimum aligned cascade), where M_1 is the number of modulators per subarray in stage 1 and d_1 is the modulator spacing, we can rewrite the stage 1 deflection angle as $\bar{\theta}_1 = (n/M_1)(\lambda/d_1)$. This reformulation defines the stage 1 deflection angle in terms of its modulator spacing d_1. Now Eqs. (A1) and (A2) can be used to determine the corresponding phase increments ($\Delta\varphi_1$ and $\Delta\varphi_2$) and the reduced phase shifts ($\hat{\varphi}_{1m}$ and $\hat{\varphi}_{2m}$) for all the modulators in both stages. The results are summarized in Table 2. Note that the generalized angles given above are specifically defined as $\bar{\theta}_1 \equiv \sin(\theta_1)$ and $\bar{\theta}_2 \equiv \sin(\theta_2)$, where θ_1 and θ_2 are the true angles.

B. *Discrete–Offset-Bias Programming of an Aligned Cascade*

Under the discrete–offset-bias protocol, both stages are programmed to deflect the incident beam by the full angle of $\bar{\theta}_S = Q(\lambda/d_2)$ so that $\bar{\theta}_1 = \bar{\theta}_2 = \bar{\theta}_S$. In terms of their respective modulator widths d_1 and d_2, the deflection angles to be generated by the two stages can be written as $\bar{\theta}_1 = (Q/M_1)(\lambda/d_1)$ and $\bar{\theta}_2 = Q(\lambda/d_2)$, and Eqs. (A1) and (A2) can be invoked to determine the specific reduced phases of each modulator in both arrays. These results are also summarized in Table 2. Note that the reduced phase shift of the mth modulator in the offset-bias stage (stage 2), given by $\hat{\varphi}_{2m} = [2\pi Q m] \bmod 2\pi$, can be simplified to $\hat{\varphi}_{2m} = [2\pi r m] \bmod 2\pi$ by use of the decomposition $Q = n + r$ and elimination of the integer multiple term $(2\pi n m)$ in the modulo operand. Hence the reduced phases for the offset-bias stage are functionally identical to those of the fine stage under the coarse–fine protocol for the specified aligned phased-array cascade. This shows the surprising fact that stage 2 has the same reduced-phase programming when either protocol for this cascade arrangement is used.

Appendix B: Diffraction Efficiency of an Aligned Two-Stage Phased-Array Deflector

The theoretical computation of the DE versus the deflection angle for an aligned two-stage phased-array cascade is determined below for both types of cascade programming. Even though the coarse–fine

Table 2. Summary of the Phase Programming Formulas for an Aligned Two-Stage Phased-Array Deflector Using Either the Coarse–Fine Protocol or the Discrete–Offset-Bias Protocol (n = integer-valued, r = real-valued, and Q = n + r)

Parameter		Protocol	
		Coarse–Fine	Discrete–Off-Set Bias
Total deflection angle	$\bar{\theta}_S$	$(n+r)(\lambda/d_2)$	$Q(\lambda/d_2)$
Stage 1		Coarse Deflector	Discrete Deflector
Deflection angle	$\bar{\theta}_1$	$n(\lambda/d_2)$	$Q(\lambda/d_2)$
Phase increment	$\Delta\varphi_1$	$2\pi(n/M_1)$	$2\pi(Q/M_1)$
Reduced phase of mth modulator	$\hat{\varphi}_{1m}$	$[2\pi(n/M_1)m]\text{mod } 2\pi$	$[2\pi(Q/M_1)m]\text{mod } 2\pi$
Stage 2		Fine Deflector	Offset-Bias Phases
Deflection angle	$\bar{\theta}_2$	$r(\lambda/d_2)$	$Q(\lambda/d_2)$
Phase increment	$\Delta\varphi_2$	$2\pi r$	$2\pi Q$
Reduced phase of mth modulator[a]	$\hat{\varphi}_{2m}$	$(2\pi rm)\text{mod } 2\pi$	$(2\pi Qm)\text{mod } 2\pi$

[a] $\hat{\varphi}_{2m}$ is the same for both protocols because $(2\pi Qm)\text{mod } 2\pi = (2\pi rm)\text{mod } 2\pi$.

cascade can be used with a more general cascade architecture, we restrict this comparative analysis to an aligned configuration of the form shown in Fig. 4 because this is the arrangement required for the discrete–offset-bias protocol. The results are represented graphically in the plot in Fig. 12.

1. Diffraction Efficiency under Coarse–Fine Programming

Under coarse–fine programming the two stages in the phased-array cascade behave as independent deflectors approximating smooth prisms with stepped phase profiles. The quantization errors in both stages cause a reduced DE, and the total DE of the cascaded deflector is equal to the DE's of the individual stages multiplied together. Each stage can be modeled as a single phased-array deflector (i.e., as an echelon grating) that has a diffraction efficiency given by the element-factor term of Eq. (5). The element factor is a function of both the modulator fill factor and the programmed deflection angle of the given phased array.

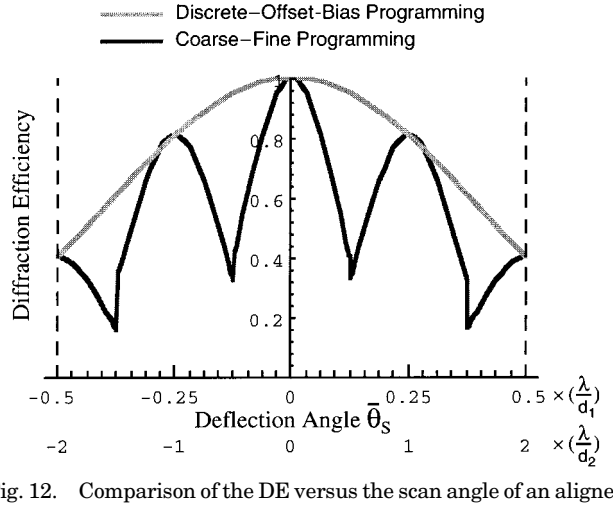

Fig. 12. Comparison of the DE versus the scan angle of an aligned two-stage phased-array deflector cascade by use of the discrete–offset-bias protocol (upper curve) and the coarse–fine protocol (lower curve). Cascade configuration: $M_1 = 4$, $M_2 = 8$, 100% filled apertures; minimum control-line arrangement (Fig. 4).

The individual stages of the aligned cascade are programmed as coarse and fine deflectors following the procedure outlined in Appendix A. For deflection by a total angle of $\bar{\theta}_S = (n + r)(\lambda/d_2)$, where n is an integer and r is real valued ($|r| \leq 0.5$), the coarse and the fine stages are programmed with generalized deflection angles of $\bar{\theta}_1 = n(\lambda/d_2)$ and $\bar{\theta}_2 = r(\lambda/d_2)$, respectively. The DE's of the individual stages, η_{course} and η_{fine}, are found by the application of Eq. (5) to each stage with the appropriate fill factor and phase increment. The total DE is equal to the DE of the individual stages multiplied together. The total DE $\eta_{\text{TOT}}{}^{\text{C–F}}$ of a two-stage phased-array deflector programmed with the coarse–fine protocol can be written as

$$\eta_{\text{TOT}}{}^{\text{C–F}} = \eta_{\text{coarse}}\eta_{\text{fine}} = \left(\frac{w_1}{d_1}\right)^2 \text{sinc}^2\left[\left(\frac{w_1}{d_1}\right)\left(\frac{\Delta\varphi_1}{2\pi}\right)\right] \times \left(\frac{w_2}{d_2}\right)^2 \text{sinc}^2\left[\left(\frac{w_2}{d_2}\right)\left(\frac{\Delta\varphi_2}{2\pi}\right)\right], \tag{B1}$$

where (w_1/d_1) and (w_2/d_2) represent the fill factors and $\Delta\varphi_1$ and $\Delta\varphi_2$ the programmed phase increments for stages 1 and 2, respectively, and $\text{sinc}(\mu) \equiv \sin(\pi\mu)/(\pi\mu)$. For a total deflection angle of $\bar{\theta}_S = (n + r)(\lambda/d_2)$, the corresponding phase increments for stages 1 and 2 in an aligned configuration are $\Delta\varphi_1 = 2\pi(n/M_1)$ and $\Delta\varphi_2 = 2\pi r$ (from Table 2), respectively, where M_1 is the number of modulators per subarray in stage 1. The values for n and r are derived from the the angle $\bar{\theta}_S$ by Eq. (A3). The maximum DE occurs when there is no deflection and has the value $(w_1/d_1)^2(w_2/d_2)^2$. The DE in Eq. (B1) varies in a discontinuous way with the deflection angle because the integer parameter n is a nonlinear, discontinuous function of the deflection angle $\bar{\theta}_S$. As $\bar{\theta}_S$ increases, the integer value n (hence $\Delta\varphi_1$) for the coarse stage remains constant, while the fine deflector scans smoothly from $r = -0.5 - +0.5$ (i.e., $\Delta\varphi_2 = -\pi - \pi$), and then n jumps to its next value of $n + 1$. The discontinuous and nonmonotonic intensity behavior of the coarse–fine programming scheme is demonstrated in the example plotted in Fig. 12.

2. Diffraction Efficiency under Discrete–Offset-Bias Programming

Using the discrete–offset-bias protocol causes the DE of the aligned two-stage phased-array deflector to be dictated primarily by the first stage (the discrete stage) because it is the only stage to exhibit phase-quantization errors. Under this programming strategy the terms AF_1 and AF_2 in Eq. (8a) are guaranteed to be at their peak values ($AF_1 = AF_2 = 1$) at $\bar{\theta}_S$ and the deflector DE is described simply by the element factor term EF_1 in Eq. (7b). The aligned two-stage phased-array system behaves like a phase-staggered version of a large, single-stage phased-array deflector that has modulators of width d_1, an effective fill factor (w_1/d_1), and a functional equivalent of M_1M_2 modulators. It is assumed here that all the light passing through the first stage (the discrete scanner) subsequently passes through the second stage (the offset-bias stage) without further attenuation, so the full two-stage device can be modeled with the simple fill factor (w_1/d_1) determined by stage 1. (This is a reasonable assumption for two-stage cascades implemented by use of a butt-coupled pair of identical phased arrays, as in our experiments.)

Under discrete–offset-bias programming both stages are programmed for deflection directly to the selected angle $\bar{\theta}_S$, which can be written as $\bar{\theta}_S = Q(\lambda/d_2)$, where Q is a real-valued constant and λ and d_2 are as previously defined. The DE of this cascade is determined solely by the term EF_1 [Eq. (7b)], which can be rewritten in terms of the fill factor and the phase increment for stage 1. The resulting total DE $\eta_{TOT}{}^{D\text{–}OB}$ of an aligned two-stage phased-array cascade programmed with the discrete–offset-bias protocol can be written as

$$\eta_{TOT}{}^{D\text{–}OB} = \left(\frac{w_1}{d_2}\right)^2 \operatorname{sinc}^2\left[\left(\frac{w_1}{d_1}\right)\left(\frac{\Delta\varphi_1{}'}{2\pi}\right)\right]. \qquad \text{(B2)}$$

Here w_1 is the clear aperture of the modulators in stage 1, d_1 is the width of these modulators, and stage 1 has a phase increment of $\Delta\varphi_1{}' = 2\pi\,(Q/M_1)$ (from Table 2), where M_1 is the number of modulators per subarray in stage 1 and Q represents the unitless scan-angle parameter. Note that the stage 1 phase increment $\Delta\varphi_1{}'$ takes on a slightly different value here than it would under coarse–fine operation (see Table 2). The maximum DE under discrete–offset-bias programming is $(w_1/d_1)^2$. Because Q (hence $\Delta\varphi_1{}'$) varies smoothly with the deflection angle $\bar{\theta}_S$, it follows from Eq. (B2) that the DE of the aligned two-stage deflector operating as a discrete–offset-bias cascade is a smooth, monotonic function of the deflection angle. Equation (B2) is identical to the element-factor envelope EF_1 of the first stage, which represents the fixed upper-bound limit to the DE of the cascaded system. Hence the discrete–offset-bias mode of operation achieves the optimal DE for such an aligned phased-array cascade.

3. Comparison of Deflector Efficiencies

Figure 12 shows comparative plots of the DE versus the scan angle for an aligned two-stage phased-array deflector programmed by use of both protocols and under the assumption of the ideal case of 100% filled apertures in both stages. The aligned-cascade arrangement requires a minimum number of control lines for a given scanner resolution. A system configuration with $M_1 = 4$ channels/subarray in stage 1 and $M_2 = 8$ channels/subarray in stage 2 was used for the plots to mimic the configuration used in the experiments described in Section 6. Because the modeling assumes 100% filled modulators, the DE curves shown in Fig. 12 represent the maximum upper-bound limits on DE that can be obtained by such an aligned two-stage cascade configuration. For partially filled modulators, as in our experiments, the essential features remain the same, but the curves are broadened and vertically compressed, thus lowering the maximum possible DE.

The DE of the cascaded phased-array deflector under discrete–offset-bias programming is a smooth, monotonic function of the deflection angle and achieves an overall higher DE than does the coarse–fine programming, which exhibits discontinuous jumps in its DE versus $\bar{\theta}_S$ profile. The discontinuous jumps occur at angles falling half-way between the discrete states that can be addressed by the coarse stage (stage 1) alone, and they exhibit a low DE as a result of the large quantization errors occurring in the fine stage (stage 2) at these angles. The experimental data from our test arrays described in Section 6 exhibit these same intensity trends. Note that the large dips in the DE curve for the coarse–fine programming scheme could be reduced by an increase in the number of modulators in the fine stage, as discussed in Section 5, but at the cost of greater phased-array complexity. Because the DE profile for the discrete–offset-bias programming scheme matches the element factor of the smallest diffracting element in the system, it uniquely achieves the highest overall DE that can be obtained by an aligned two-stage phased-array deflector with a minimum control-line configuration.

This study was supported in part by the National Science Foundation and the U.S. Office of Naval Research. The authors also thank P. Soltan and M. Lasher of the Naval Research and Development Laboratories (NRaD) in San Diego, California, for their program assistance and technical support with this project.

References

1. P. F. McManamon, T. A. Dorschner, D. L. Corkum, L. J. Friedman, D. S. Hobbs, M. Holz, S. Liberman, H. Q. Nguyen, D. P. Resler, R. C. Sharp, and E. A. Watson, "Optical phased array technology," Proc. IEEE **84,** 268–298 (1996).
2. T. C. Cheston and J. Frank, "Phased array radar antennas," in *Radar Handbook*, 2nd ed., M. I. Skolnik, ed. (McGraw-Hill, New York, 1990), Chap. 7, pp. 7.1–7.82.
3. R. M. Matic, "Blazed phase liquid crystal steering," in *Laser*

Beam Propagation and Control, H. Weichel and L. F. DeSandre, eds., Proc. SPIE **2120,** 194–205 (1994).
4. R. A. Meyer, "Optical beam steering using a multichannel lithium tantalate crystal," Appl. Opt. **11,** 613–616 (1972).
5. Y. Ninomiya, "Ultrahigh resolving electrooptic prism array light deflectors," IEEE J. Quantum Electron. **QE-9**(**8**)**,** 791–795 (1973).
6. Y. Ninomiya, "High S/N-ratio electrooptic prism-array light deflectors," IEEE J. Quantum. Electron. **QE-10,** 358–362 (1974).
7. T.-C. Lee and J. D. Zook, "Parallel array light beam deflector with variable phase plate," U.S. patent no. 3,650,602 (issued 21 March 1972).
8. C. H. Bulmer, W. K. Burns, and T. G. Giallorenzi, "Performance criteria and limitations of electro-optic waveguide array deflectors," Appl. Opt. **18,** 3282–3295 (1979).
9. D. R. Wight, J. M. Heaton, B. T. Hughes, J. C. H. Birbeck, K. P. Hilton, and D. J. Taylor, "Novel phased array optical scanning device implemented using GaAs/AlGaAs technology," Appl. Phys. Lett. **59,** 899–901 (1991).
10. F. Vasey, F. K. Reinhart, R. Houdré, and J. M. Stauffer, "Spatial optical beam steering with an AlGaAs integrated phased array," Appl. Opt. **32,** 3220–3232 (1993).
11. T. A. Dorschner and D. P. Resler, "Optical beam steerer having subaperture addressing," U.S. patent no. 5,093,740 (issued 3 March 1992).
12. J. A. Thomas and Y. Fainman, "Programmable diffractive optical element using a multichannel lanthanum-modified lead zirconate titanate phase modulator," Opt. Lett. **20,** 1510–1512 (1995).
13. P. J. Talbot and Q. W. Song, "Design and simulation of PLZT-based electro-optic phased array scanners," Opt. Memory Neural Net. **3,** 111–117 (1994).
14. T. Tatebayashi, T. Yamamoto, and H. Sato, "Electro-optic variable focal-length lens using PLZT ceramic," Appl. Opt. **30,** 5049–5055 (1991).
15. N. A. Riza and M. C. DeJule, "Three-terminal adaptive nematic liquid-crystal lens device," Opt. Lett. **19,** 1013–1015 (1994).
16. J. G. Skinner, "Optimal electrooptic deflection scheme," Appl. Opt. **7,** 1239–1240 (1968).
17. H. J. Boll, "Cascaded light beam deflector system," U.S. patent no. 3,544,200 (issued 1 December 1970).
18. T. C. Lee and J. D. Zook, "Cascade operation of light beam deflectors by fly's eye lenses," Appl. Opt. **10,** 1965–1966 (1971).
19. K. M. Flood, B. Cassarly, C. Sigg, and J. M. Finlan, "Continuous wide angle beam steering using translation of binary microlens arrays and a liquid crystal phased array," in *Computer and Optically Formed Holographic Optics,* I. Cindrich and S. H. Lee, eds., Proc. SPIE **1211,** 296–304 (1990).
20. J. A. Thomas, M. E. Lasher, Y. Fainman, and P. Soltan, "PLZT-based dynamic diffractive optical element for high-speed random-access beam steering," in *Optical Scanning Systems: Design and Applications*, L. Beiser and S. F. Sagan, eds., Proc. SPIE **3131,** 124–132 (1997).
21. G. H. Haertling, "PLZT electrooptic materials and applications—a review," Ferroelectrics **75,** 25–55 (1987).
22. R. Fleischmann and A. Lohmann, "Die Bestimmung einer absoluten Lichtphase durch Intensitätsmessung in der Beugungsfigur eines Gitters," Z. Physik **137,** 362–375 (1954).